SIAM Review
Vol. 52, No. 4, pp. 747–767

An Introduction to Fluid-Structure Interaction: Application to the Piston Problem*

Emmanuel Lefrançois†
Jean-Paul Boufflet‡

Abstract. Structure and fluid models need to be combined, or *coupled*, when problems of fluid-structure interaction (FSI) are addressed. We first present the basic knowledge required for building and then evaluating a simple coupling. The approach proposed is to consider a dedicated solver for each of the two physical systems involved. We illustrate this approach by examining the interaction between a gas contained in a one-dimensional chamber closed by a moving piston attached to an external and fixed point with a spring. A single model is introduced for the structure, while three models of increasing complexity are proposed for the fluid flow solver. The most complex fluid flow model leads us to the arbitrary Lagrangian Eulerian (ALE) approach. The pros and cons of each model are discussed. The computer implementations of the structure model, the fluid model, and the coupling use MATLAB scripts, downloadable from either http://www.utc.fr/∼elefra02/ifs or http://www.hds.utc.fr/∼boufflet/ifs.

Key words. fluid-structure interaction, mass-spring dynamics, one-dimensional fluid flow, finite elements, energy conservations, mesh deformation

AMS subject classifications. 74F10, 65C20, 76M10, 76N15

DOI. 10.1137/090758313

1. Introduction.

Easy and inexpensive access to computing capacities that would have been unthinkable a few years ago has awakened an interest in fluid-structure interaction (FSI). This branch of mechanics looks at the nonstationary coupling between a fluid flow and a flexible mechanical structure. The nonstationary aspect is due to the exchange of momentum and energy that occurs during this coupling process. There is no guarantee that stationary equilibrium conditions will be perfectly satisfied: turbulence and the dynamics of the structure may, for example, have an impact. The interaction between the sail of a boat or a plane and the surrounding aerodynamic flow, between a bridge and the wind (cf. the tragic destruction of the Tacoma Narrows Bridge in 1940), and between vessels and blood flows are all practical and challenging examples of FSI [17].

The general equation for FSI results from applying the *fundamental principle of dynamics* (FPD), or Newton's second law, to the mechanical system

$$m\vec{\Gamma} = \sum_{\text{forces}} \vec{F}_i, \tag{1.1}$$

*Received by the editors May 7, 2009; accepted for publication (in revised form) February 2, 2010; published electronically November 8, 2010.
http://www.siam.org/journals/sirev/52-4/75831.html

†Université de Technologie de Compiègne, UMR CNRS, 6253 Roberval, France (emmanuel.lefrancois@utc.fr).
‡Université de Technologie de Compiègne, UMR CNRS, 6599 Heudiasyc, France (Jean-Paul.Boufflet@utc.fr).

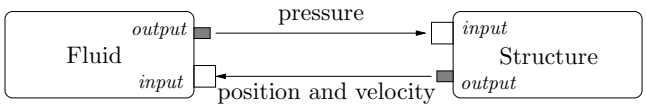

Fig. 1.1 *Principle of FSI.*

with m the system mass, $\vec{\Gamma}$ the acceleration vector, and $\vec{F}_i$ the applied forces (e.g., gravity, aerodynamics). A simple approach consists in associating a specialized *solver* with each part of the equation, using a coupling technique to provide the equality term, thus (1.1) can be broken down as follows:

Left term: computed with a structure solver.

Right term: computed with a fluid flow solver.

Equality: a coupling scheme to update common data between the solvers.

With this kind of coupling we need to identify the common data that are input and output for each of the solvers. In the case of an FSI calculation, the data exchanged correspond to the parietal pressure and the position and velocity field of the mechanical system (see Figure 1.1).

Historically, numerical models were first used for studying the elastic behavior of flexible structures. Fluid flow computations are more complex, owing to convective and turbulence effects, for example. Different approximation levels can be used, according to the level of precision required. In all cases, caution is necessary when coupling structure and fluid solvers. Mass, momentum, and energy conservation must be respected between the terms of (1.1); this is not automatically the case when distinct solvers are used to compute the left and right terms. These criteria provide the main basis for checking the quality of FSI calculations.

Our aim is to provide a basic but solid grasp of the numerics underlying the physics of FSI. Different fluid *models* are considered and compared. We shall be using the following application as an illustration: the interaction between a gas contained in a one-dimensional (1D) chamber closed by a moving piston (see Figure 2.1).

Solving the problem will require the following:

1. A structural model to solve the dynamics of the piston. At any given time the input is the fluid pressure exerted on its section by the enclosed air, and the outputs are the piston's position and velocity.
2. A fluid flow model to calculate the changing pressure on the piston. The inputs are the piston's position and velocity, and the output is the fluid pressure.

Solving any physical problem using numerical tools on a computer is part of a more general process that can be summarized as follows:

1. Constructing a *physical model*: this consists of listing the unknown variables, with the aims of defining the geometry of the system to be studied, the boundary conditions, and the physical properties, and of establishing simplifying hypotheses (e.g., stationary or not, 1, 2, or 3 dimensions, and the type of physics—solids, fluid mechanics, or thermics) [3].
2. Constructing the *mathematical model*: this is the mathematical formulation. of the relations governing the mechanical equilibrium [7].
3. Constructing the *numerical model* using finite difference, finite volume, or finite element methods, for example [8]. The numerical model consists of a system of algebraic equations to be solved [6].
4. Developing a *computer model* in order to solve the numerical model with a large number of unknowns [1].

Each step of this process deals with the same problem, but each uses its own *language*. What is called *pressure* in the physical model is denoted by the variable $p(x,t)$ in the mathematical model, by the *nodal* indexed variable p_i^n (located at the discrete x_i position at indexed time n) in the numerical model, and ultimately by a set of memory addresses in the computer model.

Three fluid models of increasing complexity are considered: the classical steady state gas law with the adiabatic assumption [21], the piston analogy [2], and the general equations governing a 1D compressible flow based on the finite element method. In order to check the quality of coupling and to compare the different models, indicators of mass, momentum, and energy conservation are systematically calculated. The computer model consists of scripts written in the MATLAB[1] language, downloadable from the personal web pages of both authors.

The following three sections present the physical, mathematical, and numerical models, respectively. Section 5 describes the mass, momentum, and energy conservation criteria used to evaluate the quality of the coupling. In section 6 we briefly present the computer model. We comment on results and list the pros and cons for each fluid model in section 7. A final section concludes this paper.

The paper requires a basic knowledge of

- mathematical techniques including differential equations and linear algebra [6, 7],
- the *FPD* and energy interpretation [18, 19],
- thermodynamics [24],

and master-level knowledge of

- concepts and equations in fluid mechanics [25],
- the finite difference method for time discretization [27],
- the finite element method (in 1D) for space discretization [8].

2. Physical Model: Description of the Application. As illustrated in Figure 2.1 we consider a gas contained in a 1D chamber [23], closed on its right-hand side by a moving piston and on its left by a fixed wall. The piston is of mass m_p and attached to an external fixed point with a spring (of rigidity k_p). The spring is defined by three different lengths, namely, unstretched (L_{so}), at rest under pressure (L_{se}), and at a given time t during the FSI process ($L_s(t)$). The current displacement, velocity, and acceleration of the piston are, respectively, given by $u(t)$, $\dot{u}(t)$, and $\ddot{u}(t)$ with regard to its position at rest.

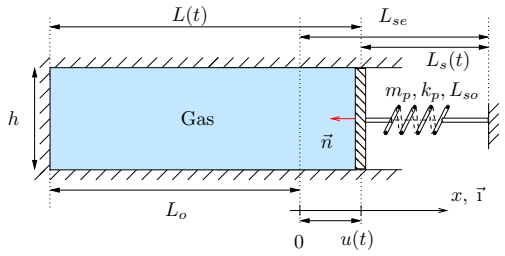

Fig. 2.1 *A gas enclosed in a chamber with a moving piston.*

[1]Scientific programming language developed by The MathWorks.

The contained gas is air. All fluid variables are taken to be uniform for any section of the chamber (1D assumption) and are consequently only x- and t-dependent. The fluid is defined by its volumic mass ρ, velocity v, pressure p, and temperature T, as well as by certain thermodynamic properties that will be described later. The air is initially at rest at pressure p_o. We assume that there are no thermic flows between the gas and the chamber: the process is taken to be *adiabatic*. The dimensions of the chamber correspond to its height h and its length, defined as L_o at rest and $L(t) = L_o + u(t)$ at time t.

The objective is to study the effect of the enclosed and compressible air on the dynamic piston response. Various piston masses are considered, to illustrate how the fluid flow model needs to be chosen carefully, according to its frequency response.

3. Mathematical Models: The Governing Equations.

3.1. Structure Part. The piston motion is governed by (1.1). For a movable piston with only one *degree of freedom* (i.e., unknown), $u(t)$ can be written as [15, 18, 19]

$$m_p\ddot{u} = -k_p(L_s(t) - L_{so})\vec{n}.\vec{\imath} + Ap(t), \tag{3.1}$$

with A the piston section, $L_s(t) = L_{se} - u(t)$ the current length, $\vec{\imath}$ the unity vector on the x-axis, and $\vec{n} = -\vec{\imath}$ the piston normal vector. The right-hand side of (3.1) represents the restored force of the spring and the fluid pressure exerted on the piston. The static position at rest is defined by $u = \dot{u} = \ddot{u} = 0$ for $p = p_o$. We deduce from (3.1) that

$$k_p(L_{se} - L_{so}) + Ap_o = 0 \quad \text{with} \quad p_o = \text{chamber pressure at rest.} \tag{3.2}$$

Substituting (3.2) into (3.1), we finally obtain

$$m_p\ddot{u} + k_p u(t) = A(p(t) - p_o), \quad \text{with} \quad u(0) = u^0 \text{ and } \dot{u}(0) = 0, \tag{3.3}$$

the classical form of a mass-spring system completed by initial conditions on $u(0)$ and $\dot{u}(0)$. We define $f_o = \frac{1}{2\pi}\sqrt{\frac{k_p}{m_p}}$ as the natural frequency (Hz) and $\mathcal{T}_o = \frac{1}{f_o}$ as the natural period (sec) of the mass-spring system. At this stage this mathematical model is incomplete: the pressure $p(t)$ exerted on the piston is unknown. This term may only be calculated by a fluid flow model that must be *coupled* to the piston model (see (3.3)).

3.2. Fluid Part. Three models of increasing complexity are presented for computing the pressure term $p(t)$ in (3.3).

3.2.1. A-Model: Ideal Gas Law with Adiabaticity Condition. The internal pressure in the chamber is assumed to be homogeneous (not x-dependent) and directly dependent on the piston motion. The compressive process is assumed to be adiabatic: there are no exchanges between the fluid and its external environment. The change in pressure $p(t)$ is consequently governed by the adiabatic *ideal gas law* [24],

$$p(t)V(t)^\gamma = p_o V_o^\gamma \quad \text{or} \quad \frac{p(t)}{\rho(t)^\gamma} = \frac{p_o}{\rho_o^\gamma}, \quad \text{with} \quad p(t) = \rho(t)\mathcal{R}T(t). \tag{3.4}$$

$V(t) = V_o + Au(t)$ defines the current volume of gas, $T(t)$ and $\rho(t)$ are the temperature and the volumic mass of the gas, $\mathcal{R}$ is the individual gas constant, and $\gamma = 1.4$ is the specific heat ratio of the gas. Terms with an o subscript refer to conditions at rest.

The homogeneity assumption (not x-dependent) is only valid for low piston speeds, and it is therefore assumed that the fluid adapts itself instantaneously.

REMARK 1. *For this model, it is not possible simply to consider the case of a fixed temperature (Boyle–Mariotte law,* 1662*, that stipulates $p(t)V(t)$ is kept constant). This approach is in contradiction with the adiabatic assumption of the physical model presented: thermic flows are indeed vital for maintaining a fixed temperature for a Boyle–Mariotte process.*

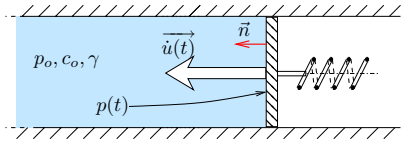

Fig. 3.1 *Piston analogy in a semi-infinite chamber.*

3.2.2. B-Model: Piston Analogy Model. This model gives an analytical relation for the variation in pressure resulting from the displacement of a piston in a semi-infinite chamber [2, 21]. The concept is illustrated in Figure 3.1. The *exact* pressure exerted on the moving piston is then given by

$$p(t) = p_o \left(1 + \frac{\gamma - 1}{2}\left(\frac{\overrightarrow{\dot{u}(t)}.\vec{n}}{c_o}\right)\right)^{\frac{2\gamma}{\gamma-1}}, \tag{3.5}$$

where p_o and c_o are, respectively, the pressure and the speed of sound of the ambient conditions in front of the wave generated by the piston and $\gamma = 1.4$ is the specific heat ratio of the gas. The B-model, however, can only be used to calculate the pressure on the piston, and not at any point in the chamber.

REMARK 2. *This relation holds when there is a single simple wave (with no reflective wave due to inappropriate boundary conditions, for example).*

3.2.3. C-Model: 1D Compressible Fluid Flow Evolution. This model is based on a set of three coupled equations [7, 13, 21, 23] governing the nonstationary evolution of a compressible 1D flow.

General 1D Fluid Flow Equations for a Fixed Domain. For a fixed domain of constant length L, these equations correspond to the conservation laws

$$\begin{aligned}
&\text{mass:} && \frac{\partial \rho}{\partial t} + \frac{\partial \rho v}{\partial x} = 0, \\
&\text{momentum:} && \frac{\partial \rho v}{\partial t} + \frac{\partial (\rho v^2 + p)}{\partial x} = 0 \quad \text{for all } x \in [0,\ L],\ t \geq 0, \\
&\text{total energy:} && \frac{\partial \rho e}{\partial t} + \frac{\partial (\rho e + p)v}{\partial x} = 0.
\end{aligned}$$

All the variables are (x, t)-dependent, but this notation has been suppressed for clarity. The total volumic energy $e(x, t)$ is given by

$$e = C_v T + \frac{v^2}{2}, \quad \text{with} \quad C_v = \frac{\mathcal{R}}{\gamma - 1}, \quad \gamma = 1.4, \quad \text{and} \quad \mathcal{R} = 287\ \mathrm{m^2 s^{-2} K^{-1}}.$$

C_v is the specific heat capacity of the gas in a constant volume process, and $\mathcal{R}$ the individual gas constant. The local pressure $p(x,t)$ is related to the temperature $T(x,t)$ according to the ideal gas law:

$$p = \rho \mathcal{R} T = (\gamma - 1)\left(\rho e - \frac{1}{2}\rho v^2\right).$$

No viscous effects are considered. These three equations are usually combined in a vectorial form such as

$$\frac{\partial}{\partial t}\{U\} + \frac{\partial}{\partial x}\{F\} = \{0\}, \text{ with } \{U\} = \begin{Bmatrix} \rho \\ \rho v \\ \rho e \end{Bmatrix} \text{ and } \{F\} = \begin{Bmatrix} \rho v \\ \rho v^2 + p \\ (\rho e + p)v \end{Bmatrix}, \tag{3.6}$$

that is rewritten in an indicial form:

$$\frac{\partial U_i}{\partial t} + \frac{\partial F_i}{\partial x} = 0 \text{ for } i = 1, 2, 3. \tag{3.7}$$

The index i is related to the form corresponding to the mass ($i = 1$), momentum ($i = 2$), and energy ($i = 3$) conservation, respectively.

The term $\{F\}$ is related to a transport phenomenon: it is known as the *flux* term. The flux $F(q)$ of any quantity q (e.g., mass, momentum, and energy) is defined as *the quantity flowing through a section S per unit time*. For a fixed section, it is related to the local fluid velocity:

$$F(q) = \int_S q\vec{v}.\vec{n}dS, \tag{3.8}$$

where $\vec{n}$ defines the orientation vector of the section (along the x-axis in this case).

Notion of Movable Domains. The finite element method [8, 10, 30, 31, 32] is used to solve the fluid flow equations. This involves computing the solution at discrete locations, called *nodes*, within the fluid domain; two successive nodes form a *finite element*. The calculation domain is called a *mesh* and is illustrated in Figure 3.2. The two-node *finite elements* are also shown and numbered using parentheses. A node attached to a movable boundary (such as the piston at $x = L(t)$) must follow it. In order to prevent nodes impinging or traversing, interior nodes must be moved, except for the node attached to the fixed boundary located at $x = 0$. This is similar to the compression or expansion of the bellows of an accordion.

Unfortunately, (3.7) is not valid for movable nodes: the flow term F_i must be corrected to take into account the motion of the nodes where it is calculated. We then consider that any point of the fluid domain is movable at a given velocity $w_x(x,t)$. This concept of moving coordinates is illustrated in Figure 3.3.

The chamber is superimposed as straight lines, respectively, for two successive times t and $t + \Delta t$. We consider a *mesh* composed of five *nodes* located at regular intervals along the domain and indexed from 1 through 5. They are represented by

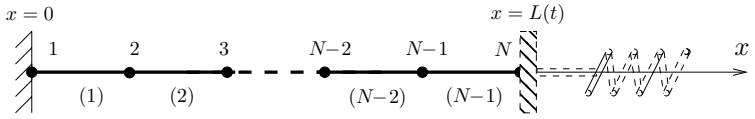

Fig. 3.2 *Fluid mesh composed of N nodes and Nelt = N − 1 two-node finite elements.*

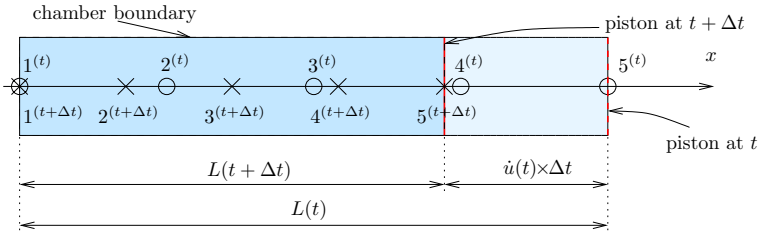

Fig. 3.3 *Moving physical space $x(t)$ representation.*

- a circle symbol ($\circ$) to depict their position at time t;
- a cross symbol ($\times$) to depict their position at time $t+\Delta t$.

It is clearly essential to be able to move nodes in order to prevent the traversing node effect, visible in Figure 3.3 between nodes 4 and 5: if nodes 4 and 5 are fixed, then finite element (4) is outside the domain at $t+\Delta t$.

Fluid Flow Formulations. At this stage two classical formulations based on the relations between the *observer attached to a node* and the fluid particles can be harnessed to express the fluid flow relations:

- *Eulerian*: the observer is fixed ($w_x(x,t)=0$) and sees the particles passing.
- *Lagrangian*: the observer is attached to the fluid particle ($w_x(x,t)=v(x,t)$).

The set of equations (3.7) corresponds to the Eulerian approach. The Lagrangian approach is essentially used for closed domains for which there are no inflow or outflow conditions (the same particles can be observed throughout the process). In the general case of a flow in a duct, the Lagrangian approach suffers from the limitation that any particle leaving the domain (outflow) must be replaced by a new one (inflow). A third formulation is proposed for general cases of fluid flow, based on a combination of the Eulerian and Lagrangian approaches and known as the ALE (*arbitrary Lagrangian Eulerian*) approach [11, 12].

Correctly calculating the flows passing through a moving section at velocity w_x is vital for ensuring the conservation of mass, momentum, and energy. This is illustrated in Figure 3.4 via an electrical analogy, namely, the measurement in a cable of the flow of electrons passing through a movable probe. Three different cases are considered: a fixed probe (Eulerian), a movable probe at electron velocity (Lagrangian), and finally a probe moving in opposite directions (ALE). Measures are illustrated with an ammeter-type graduation at the top of the probe. The measured flow is then a function of the *gauge* velocity of the particle with respect to the probe motion. For a movable section at velocity w_x (see Figures 3.4 (b) and (c)), the flow through this section, given by (3.8), is corrected as follows to take into account the section motion

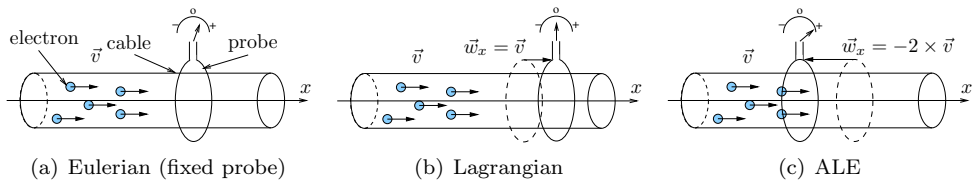

(a) Eulerian (fixed probe) (b) Lagrangian (c) ALE

Fig. 3.4 *Electrical analogy for flow measurement according to probe motion.*

(gauge velocity):

$$\tilde{F}(q) = \int_S q(\vec{v} - \vec{w}_x).\vec{n}dS.$$

Note that if $\vec{w}_x = \vec{v}$, the measured flow equals zero: the observer attached to the moving node sees no particles passing.

General 1D fluid flow equations for the ALE formulation. Applying the same *corrective* strategy to the vector form given by (3.7) leads to

$$\frac{\partial}{\partial t}(JU_i) + J\frac{\partial}{\partial x}(\underbrace{F_i - w_x U_i}_{\tilde{F}_i}) = 0 \text{ for } i = 1, 2, 3. \tag{3.9}$$

The second term $\tilde{F}_i$ in the spatial derivative is the corrected flow with respect to the movable space coordinate. U_i, F_i remain fixed (see (3.7)), and $w_x(x,t)$ defines the local domain velocity.

This set of equations is placed in a fixed space denoted by ξ (belonging to $[0,\ L_o]$) in order to make the mathematical integration easier. The $J(x,t)$ variable appearing in (3.9) is called the *Jacobian* and is related to the substitution rule between $x(t)$ and ξ. It is defined by

$$J(x,t) = \frac{dx(\xi,\ t)}{d\xi} \quad \text{or} \quad \frac{d}{dx} = J\frac{d}{d\xi} \quad \text{such that} \quad \int_{x(t)} f(x,t)dx = \int_\xi f(x(\xi),t)Jd\xi.$$

REMARK 3. *This form is general, covering both the Eulerian formulation by considering* $w_x(x,t) = 0$ *and the Lagrangian approach by considering* $w_x(x,t) \equiv v(x,t)$, *for all* (x,t). *The ALE approach combines the best features of both the Lagrangian description (tracking free surfaces and interfaces between different materials are typical examples) and the Eulerian description. The ALE approach allows the nodes on the computational grid to move in any prescribed manner, and herein lies the power of the ALE approach.*

Boundary conditions are given by a zero-flow condition at $x = 0$ and by ensuring kinematic compatibility between fluid flow and piston velocity at $x = L(t)$, that is,

$$v(0,t) = 0 \quad \text{and} \quad v(L(t),t) = \dot{u}(t) \text{ for } t \geq 0.$$

4. Numerical Models. Numerical techniques with an increasing level of complexity are described in this section, from the classical scalar differential equation for the structure solver to the finite element approach for the C-model fluid flow solver.

4.1. Structure Solver. The time resolution of the scalar (3.3) is ensured using an implicit finite difference [27] Newmark–Wilson scheme. It is based on the following time series expansions on u and $\dot{u}$:

$$u^{n+1} = u^n + \Delta t\dot{u}^n + \frac{\Delta t^2}{4}(\ddot{u}^n + \ddot{u}^{n+1}) \quad \text{and} \quad \dot{u}^{n+1} = \dot{u}^n + \frac{\Delta t}{2}(\ddot{u}^n + \ddot{u}^{n+1}). \tag{4.1}$$

The indexes $n-1$, n, and $n+1$ correspond to the times $t - \Delta t$, t, and $t + \Delta t$, as illustrated in Figure 4.1. Δt is the time step between two successive solutions. We deduce from the first relation given in (4.1) that

$$\ddot{u}^{n+1} = \frac{4}{\Delta t^2}\Delta u - \frac{4}{\Delta t}\dot{u}^n - \ddot{u}^n. \tag{4.2}$$

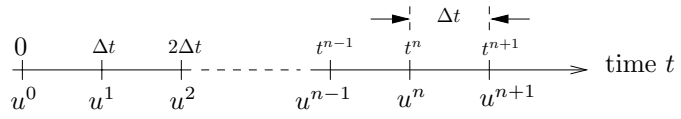

Fig. 4.1 *Time axis discretization and corresponding u solution.*

The variation $\Delta u = u^{n+1} - u^n$ between two successive times is obtained by injecting (4.1) and (4.2) into (3.3), where all structure variables are taken at time $n+1$:

$$\left(\frac{4m_p}{\Delta t^2} + k_p\right)\Delta u = A(p^n - p_o) + k_p u^n + m_p\left(\frac{4}{\Delta t}\dot{u}^n + \ddot{u}^n\right). \tag{4.3}$$

This recurrence relation allows the new piston position u^{n+1} to be computed from u^n, $\dot{u}^n$, and $\ddot{u}^n$. The structure position is then updated according to

$$u^{n+1} = u^n + \Delta u, \tag{4.4}$$

and the velocity and acceleration are also updated according to (4.1) and (4.2). The first step ($n = 1$) of (4.3) requires the initial conditions denoted by u^0 and $\dot{u}^0$ to be taken into account in order for $\ddot{u}^0$ to be deduced. It is easy to show from (3.3) that

$$\ddot{u}^0 = \frac{1}{m_p}\left(-k_p u^0 + A(p(0) - p_o)\right),$$

where $p(0)$ is the uniform pressure in the chamber resulting from an adiabatic variation entailed by the initial change in the piston position u^0.

4.2. Fluid Solver. The A- and B-models explicitly express the change in pressure as a function of the piston position. This section is devoted to the implementation of the C-model, which is the most complex of the numerical models presented. It is based on a finite element approach for spatial discretization and a Lax–Wendroff scheme [20] for temporal resolution. In order to avoid tedious mathematical developments we deliberately avoid going into too much detail here. For more details on the finite element method, we refer the reader to [8, 10, 30, 31, 32].

To summarize, the C-model based on the finite element method requires a *variational form* W of the system (3.9),

$$W = \int_0^{L_o} \psi \frac{\partial J U_i}{\partial t} d\xi - \int_0^{L_o} \frac{\partial \psi}{\partial \xi}\tilde{F}_i d\xi + \left[\psi \tilde{F}_i\right]_0^{L_o} = 0 \ \ \forall \psi(\xi) \quad \text{for } i = 1, 2, 3, \tag{4.5}$$

where $\psi(\xi)$ is any test-function of class C^1 (first derivative exists and is continuous). The integration is performed on the fixed space ($\xi \in [0,\ L_o]$) and the last two terms result from an integration by parts of the flux term.

A time integration between two successive times (indexed n and $n+1$) leads to

$$\int_0^{L_o} \psi \left(JU_i\right)^{n+1} d\xi - \int_0^{L_o} \left(JU_i\right)^n d\xi - \Delta t\left(\int_0^{L_o} \frac{\partial \psi}{\partial \xi}\tilde{F}_i^{n+\frac{1}{2}} d\xi + \left[\psi \tilde{F}_i^{n+\frac{1}{2}}\right]_0^{L_o}\right) = 0. \tag{4.6}$$

The final step is a spatial discretization on the finite elements of the mesh followed by an *assembling* process to obtain

$$[M]^{n+1}\{U_i\}^{n+1} - [M]^n\{U_i\}^n - \Delta t\{R_i\}^{n+1/2} = \{0\} \quad \text{for } i = 1, 2, 3, \tag{4.7}$$

where $\{U_i\}^n$ is the $(N \times 1)$ global vector of unknowns of the ith equation of (3.9). $[M]^{n+1}$ and $[M]^n$ are $(N \times N)$ global *mass* matrices (at times n and $n+1$). The term $\{R_i\}^{n+1/2}$ is an $(N \times 1)$ global residual vector calculated at the half-way time step. Equation (4.7) represents the system of equations to be solved for each time step [6].

REMARK 4. *At this stage, the mass matrices* $[M]^n$ *and* $[M]^{n+1}$ *are computed on the meshes deformed at times* n *and* $n+1$*, respectively. In* $1D$ *analysis the residual vector* $\{R_i\}^{n+1/2}$ *can be calculated on any mesh between times* n *and* $n+1$*, since the result of the calculation is independent of the particular mesh chosen. This is not, however, the case in* $2D$ *and* $3D$ *analyses, where a space conservation law has to be respected. We refer the reader to* [9, 12, 16, 29].

The *explicit* nature of the Lax–Wendroff scheme makes it possible to solve the three systems $(i = 1, 2, 3)$ separately for each new time step $n+1$. A *temporal stability criterion* must nevertheless be satisfied in order to prevent spurious and nonphysical oscillations that occur when the chosen time step Δt exceeds the numerical time required for information to cover a distance L^e corresponding to the length of an element. This criterion, known as the *CFL* (Courant, Friedrichs, and Levy) condition, can be written

$$\Delta t = CFL \times \min\left(\frac{L^e}{|v + c + w_x|}\right), \quad \text{with} \quad CFL < 1, \tag{4.8}$$

where $c = \sqrt{\gamma \mathcal{R} T}$ is the local speed of sound. Because of the nonpositivity of the scheme, a *shock capturing technique* [5] may be used to ensure *spatial stability* in the presence of significant convective effects (not developed here but available in the MATLAB scripts).

4.3. Fluid Mesh Deformation Technique. Fluid mesh deformation at each time step of the coupling scheme is necessary (see section 3.2.3) to

1. ensure kinematic compatibility between the fluid domain and the piston position;
2. prevent the phenomenon of traversing by fluid nodes near the piston.

Figure 4.2 illustrates two successive mesh configurations at times t and $t+\Delta t$ resulting from a positive piston motion equal to $\dot{u} \times \Delta t$, where $\dot{u}$ is the piston velocity computed by the structure solver. The new position x_j^{n+1} for node j is given by a simple linear interpolation,

$$x_j^{n+1} = x_j^n + \frac{j-1}{N-1} \times \dot{u} \times \Delta t \quad \text{for } j = 1, \ldots, N, \tag{4.9}$$

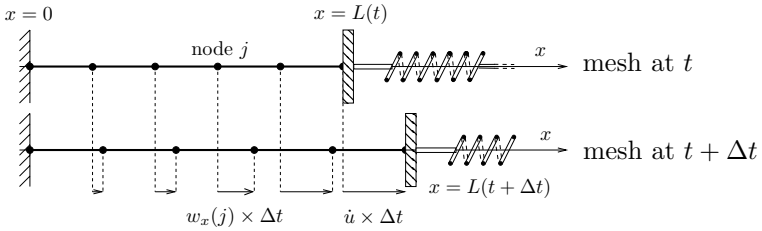

Fig. 4.2 *Fluid mesh deformation between two successive times* t *and* $t + \Delta t$.

where N is the total number of nodes for the fluid mesh. We then deduce the nodal velocity $w_x(j)$:

$$w_x(j) = \frac{x_j^{n+1} - x_j^n}{\Delta t} = \frac{j-1}{N-1} \times \dot{u} \quad \text{for } j = 1, \ldots, N. \tag{4.10}$$

5. Quality Indicators for the C-Model: Postprocessing Analysis. Three indicators are calculated to check the conservation capabilities of the ALE approach (C-model only) and the coupling scheme. All three are obtained by integrating on the domain of (3.9) with $(i = 1)$ for the mass, $(i = 2)$ for the force (or *momentum*), and $(i = 3)$ for the energy, such that

$$\frac{\partial}{\partial t} \int_0^{L(t)} U_i A dx + A \left[F_i - w_x U_i \right]_0^{L(t)} = 0. \tag{5.1}$$

The flux term has been modified using the divergence theorem.

Considering the definitions of U_i and F_i given by (3.6) and the boundary conditions $(v(L(t)) = w_x(L(t)) = \dot{u}(t)$ and $v(0,t) = w_x(0,t) = 0)$, we deduce from (5.1) the three following indicators.

5.1. Mass Conservation. The first component of (5.1) corresponds to the fluid mass (M_f) conservation in a closed domain:

$$\frac{\partial}{\partial t} \int_0^{L(t)} \rho A dx = 0 \quad \Rightarrow \quad M_f(t) = \int_0^{L(t)} \rho A dx = cste = M_f(0).$$

The fluid solver computes the mass $M_f(t)$ that is compared to the initial mass $M_f(0)$.

5.2. Momentum Conservation. The second component of (5.1) expresses that the fluid momentum variation results from the piston force:

$$\frac{\partial}{\partial t} \int_0^{L(t)} \rho A v dx - p(0)A = -p(L)A \equiv -\underbrace{k_p u(t)}_{\mathcal{F}_p^s}. \tag{5.2}$$

The left-hand term (the integral) is the force $\mathcal{F}_p^f$ computed by the fluid solver and is compared to the piston force $\mathcal{F}_p^s$ computed by the structure solver.

5.3. Energy Conservation. Time integration of the third component of (5.1) between the initial condition and the current time t yields the impulsion $\mathcal{I}(t)$ corresponding to the total fluid energy variation (left-hand term) or the fluid energy required for the piston motion (right-hand term):

$$\mathcal{I}(t) = \int_0^{L(t)} \rho A e dx - \int_0^{L(0)} \rho A e dx = -\int_0^t A p(L,t) v(L,t) dt. \tag{5.3}$$

On the other hand, the time integration of (3.3) allows us to define the variation of the mechanical energy of the piston,

$$\mathcal{E}(t) - \mathcal{E}(0), \quad \text{with} \quad \mathcal{E}(t) = \frac{1}{2} m_p \dot{u}(t)^2 + \frac{k_p}{2} (L s_e - u(t) + L s_o)^2. \tag{5.4}$$

Mechanical energy is composed of a kinetic part $\mathcal{E}_c(t)$ and a potential part $\mathcal{E}_p(t)$.

Energy conservation is then ensured if

$$\mathcal{I}(t) = \mathcal{E}(t) - \mathcal{E}_o \text{ for } t \geq 0,$$

where $\mathcal{E}_o = \frac{1}{2}k_p(Ls_e - u(0) + Ls_o)^2$ results from the initial conditions. $\mathcal{I}(t)$ is computed by the fluid solver, while $\mathcal{E}(t) - \mathcal{E}_o$ is computed by the structure solver.

6. Computer Model. The coupling scheme regularly updates common data between the fluid and structure solvers, namely, the pressure and the piston position and velocity. The coupling scheme is based on a staggered time integration method [23] and is illustrated in Figure 6.1.

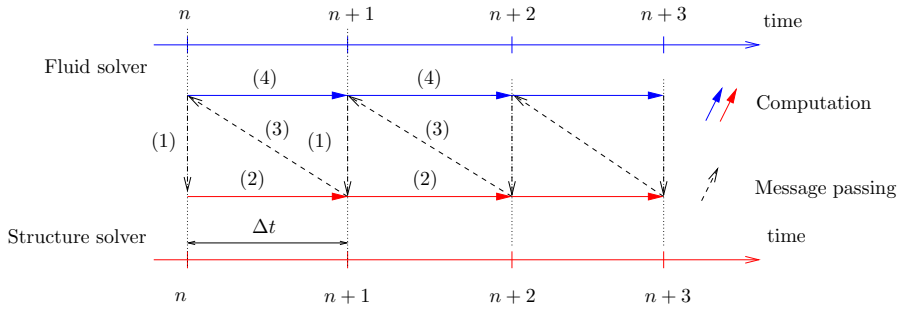

Fig. 6.1 *Coupling scheme between structure and fluid solvers.*

This coupling scheme must be read as follows:

- *Step* (1): Transfer of $p(t)$ from the fluid to the structure.
- *Step* (2): Calculation of the new piston position and velocity.
- *Step* (3): Transfer of $u(t + \Delta t)$ and $\dot{u}(t + \Delta t)$ from the structure to the fluid.
- *Step* (4): Fluid calculation for new pressure $p(t + \Delta t)$ and mesh adaptation. Go back to Step (1) until a given number of steps is reached.

The computer model was developed using MATLAB, in the form of a set of modular scripts. Documentation, including a tutorial, is available from either http://www.utc.fr/∼elefra02/ifs or http://www.hds.utc.fr/∼boufflet/ifs.

7. Practical Results. The results of 1D FSI calculations with the A-, B-, and C-model fluid flow models are presented with an emphasis on physical analysis. We also provide comparisons with derivative versions of the C-model (pure Eulerian and pure Lagrangian approaches) to illustrate the particular advantages and drawbacks of the different techniques.

General parameter values are

$$L_{so} = 1.2 \text{ m},\ L_o = 1 \text{ m},\ k_p = 10^7 \text{ N/m},\ m_p = [10, 20, 100, 1000] \text{ kg},\ u^0 = 0.20 \text{ m},$$
$$p_o = 10^5 \text{ Pa},\ T_o = 300 \text{ K},\ c_o = \sqrt{\gamma \mathcal{R} T_o} = 334.7 \text{ m/s},\ K, CFL = 0.9,\ Nelt = 100.$$

REMARK 5. *We choose the number of finite elements, denoted* $Nelt$*, by examining convergence: for different mesh sizes we measure the speed of a propagated disturbance and we select the mesh size where this velocity is closest to the theoretical speed of sound* c_o*.*

The natural piston frequency is a function of m_p (k_p is kept constant), as shown in Table 7.1.

Table 7.1 *Natural frequencies of the piston.*

m_p (kg)	1000	100	20	10
f_o (Hz)	16	50	113	159
$\mathcal{T}_o$ (s)	$6.25\ 10^{-2}$	$2\ 10^{-2}$	$8.85\ 10^{-3}$	$6.28\ 10^{-3}$

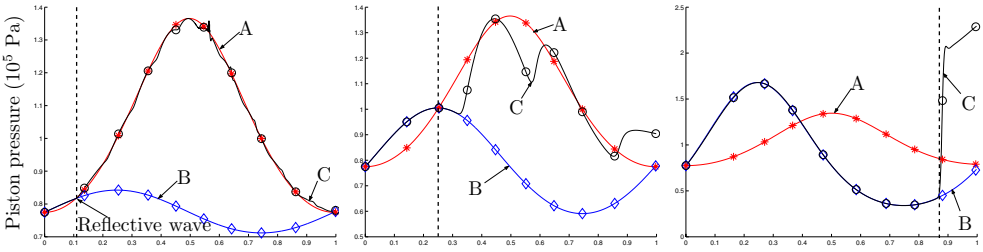

(a) $f_o = 16$ Hz. (b) $f_o = 50$ Hz. (c) $f_o = 159$ Hz.

Fig. 7.1 *A- (∗), B- (⋄), and C-models (∘): piston pressure variations.*

The following constants are used in order to normalize the results:

$$\mathcal{F}_o = k(L_{se} - u^0 - L_{so}) + Ap_o, \quad \mathcal{E}_o = \frac{1}{2}k_p(L_{se} - u^0 + L_{so})^2, \quad \mathcal{T}_o, \quad \text{and} \quad u^0,$$

respectively, for the force acting on the piston, the mechanical energy, the time, and the piston motion.

7.1. Piston Pressure. We now focus on the ability of the different fluid models to predict piston pressure.

Depending on the piston characteristics (k_m and m_p), different flow regimes may be observed. Three frequencies are considered for the (piston+spring) system: $f_o = 16$ Hz, 50 Hz, and 159 Hz.

The results are illustrated in Figures 7.1 (a), (b), and (c). The x-axis corresponds to the normalized time and the y-axis to the piston pressure. In each figure three curves are plotted: the A-, B-, and C-models are plotted with star ($*$), diamond ($\diamond$), and circle ($\circ$) symbols, respectively. A vertical dashed line is superimposed to show the time step at which the wave generated by the initial condition impacts the piston. The time step in question corresponds to the validity limit of the exact B-model (see Remark 2 in section 3.2.2). In order to analyze these results, we introduce the notion of a *characteristic time*. This can be defined in various ways:

- for the fluid it is the time required for a pressure wave to cross the chamber from one side to the other,

$$\mathcal{T}^f_{char} \approx L(t)/c_o \approx 3.6\ 10^{-3} s;$$

- for the structure it is the natural period of the piston, $\mathcal{T}^s_{char} = \mathcal{T}_o$.

If the two characteristic times are similar, the fluid and the structure *see* each other and the coupling is *strong*. In the case where one of the characteristic times significantly exceeds the other, the dynamics in question (fluid or structure) can be considered as quasi-steady for the other: the coupling is *weak*.

From Figures 7.1 (a), (b), and (c), we observe and can conclude the following:

1. In all cases, the B- and C-models correspond perfectly as long as the reflective wave has not impacted the piston (from time 0 to the time shown by the vertical dashed line). The C-model can thus be validated with respect to the "exact" behavior of the B-model.
2. The A- and C-models are in good agreement only for the lowest frequency $f_o = 16$ Hz. This can be explained in terms of *characteristic time*:
   - For $f_o = 16$ Hz, the characteristic times differ by one order of magnitude:
   $$\frac{\mathcal{T}^s_{char}}{\mathcal{T}^f_{char}} = \frac{6.25\ 10^{-2}}{3.6\ 10^{-3}} = 17.36 \quad \Rightarrow \quad \mathcal{T}^s_{char} > \mathcal{T}^f_{char}.$$
   The piston *does not see* the pressure waves: the coupling is *weak*, and the evolution *can be* seen as *quasi-steady*.
   - For $f_o = 159$ Hz, the characteristic times are of the same order:
   $$\frac{\mathcal{T}^s_{char}}{\mathcal{T}^f_{char}} = \frac{6.28\ 10^{-3}}{3.6\ 10^{-3}} = 1.75 \quad \Rightarrow \quad \mathcal{T}^s_{char} \approx \mathcal{T}^f_{char}.$$
   The coupling is *strong*, and nonstationary effects become visible.

7.2. Change in Fluid Flow within the Chamber. Figure 7.2 shows a "3D-view" of the pressure changes in the chamber for $f_o = 113$ Hz calculated with the C-model.

The x-axis corresponds to the spatial coordinate along the chamber, the y-axis corresponds to the normalized time, and the z-axis corresponds to the pressure profile in the chamber. The piston position is superimposed with a circle ($\circ$) symbol; the piston motion is clearly visible along the $x(t)$-axis with a maximum amplitude of $\pm 0.2\ m$ for this calculation.

We observe an incident pressure wave resulting from the piston's movement from its initial position u^0. This wave impacts the fixed wall at time $t/\mathcal{T}_o = 0.4$. We

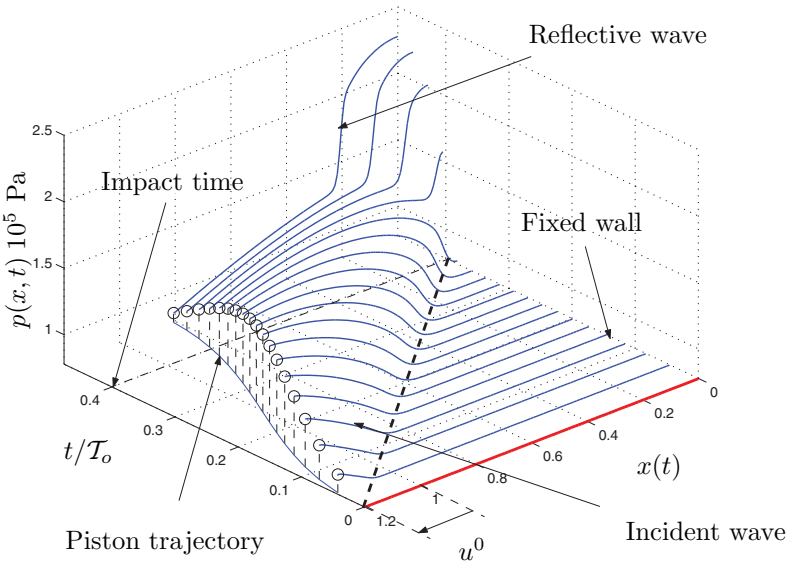

Fig. 7.2 *3D illustration of $p(x,t)$ for the C-model: $u^0 = 0.2\ m$, $f_o = 113\ Hz$.*

subsequently see a reflective wave coming back toward the piston. The velocity wave is measured by

$$c = \frac{L_o + u^0}{0.4 \times \mathcal{T}_o} = \frac{1.2}{0.4 \times 0.0089} = 337 \text{ m/s}.$$

As expected (see Remark 5), this is a good approximation of the exact speed of sound calculated with $c_o = \sqrt{\gamma \mathcal{R} T} = 334.7$ m/s. The fluid mass variation $\Delta M_f(t)/M_f(0) = 0.07\%$ confirms the quality of the ALE approach for mass conservation.

A bold dashed line depicts the incident wave path in the (x,t) space. Its slope in the (x,t) space is constant, corresponding to a wave of constant speed propagated within a fluid domain at rest and at a uniform temperature.

7.2.1. Frequency Dependent Flow Regime. Three different natural frequencies f_o (see section 3.1) of the piston were considered: $f_o = 16,\ 50$, and 159 Hz. The results are illustrated in Figures 7.3 (a), (b), and (c). The computing time is equal to half the natural period in order to avoid superimposing curves on the graph.

As in Figure 7.2, we use 3D views of the piston pressure evolution completed on piston position by a circle ($\circ$) symbol. Piston pressure changes resulting from the A- and B-models are also shown, respectively, with a star ($*$) and a diamond ($\diamond$) symbol. In each figure, the values of u^0 and $\mathcal{F}_o$ and total mass variation $\Delta M_f(t)/M_f(0)$ (only valid for the C-model) are indicated.

We observe the following:

1. The total fluid mass is perfectly conserved in spite of a piston motion that may reach 20% of the chamber length ($\Delta M_f/M_f(0) \leq 0.08\%$).
2. The fluid regime is quasi-steady (3D views) for the lowest frequency (see Figure 7.3 (a)). In this case, the fluid characteristic time is several orders of magnitude smaller than the natural period of the piston: the fluid adapts itself *instantaneously* to the piston's motion. This explains why the piston pressures given by the A- and C-models are in very good agreement ($\circ$ and $*$ symbols are almost merged in Figure 7.3 (a)).
3. The fluid regime is unsteady (transient) for the higher frequencies (Figures 7.3 (b) and (c)), thus requiring the C-model to be used.
4. The third case (Figure 7.3 (c)) leads to a strong compression phenomenon with a strong pressure gradient that may become a *shock* if the chamber length is *semi-infinite*. In case of a strong shock, a *shock capturing technique* [5] is required to ensure the stability of the numerical scheme.
5. The incident wave path (bold dashed line) is clearly visible in Figures 7.3 (b) and (c) with different slope values in (x,t) in relation to the normalized time axis (values of $\mathcal{T}_o$ differ).

7.2.2. Transfers and Conservation Considerations. Force and energy transfers are plotted in Figures 7.4 (a) and (b) for $f_o = 16$ Hz and 159 Hz. Each graph is composed of three parts (C-model results):

- *top:* normalized signals $u(t)/u^0$;
- *middle:* force $\mathcal{F}_p$ acting on the piston with square ($\square$) symbols for the value calculated by integrating fluid momentum (5.2) and circle ($\circ$) symbols for the value calculated from the elongated spring (3.1);
- *bottom:* structure energy $\mathcal{E}(t)$ with square ($\square$) symbols (from (5.4)) and fluid energy $\mathcal{I}(t)$ with circle ($\circ$) symbols (from (5.3)). Kinetic energy $\mathcal{E}_c(t)$ is also shown as a dashed line in order to illustrate structure energy transfer from potential to kinetic.

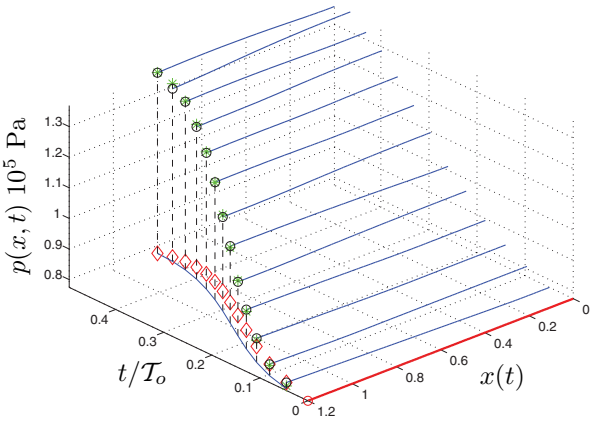

(a) $f_o = 16$ Hz, $\Delta M_f/M_f(0) = 0.02\%$.

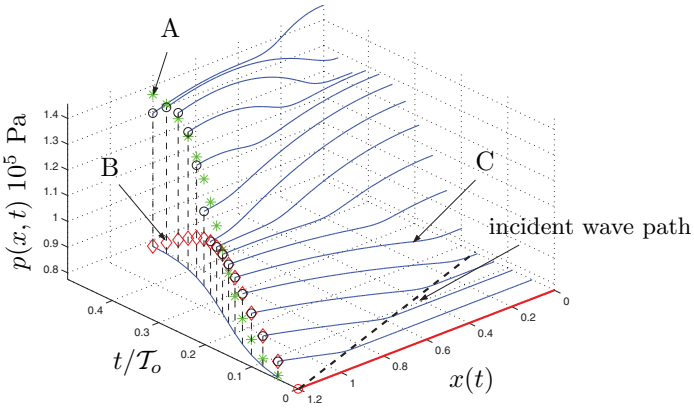

(b) $f_o = 50$ Hz, $\Delta M_f/M_f(0) = 0.04\%$.

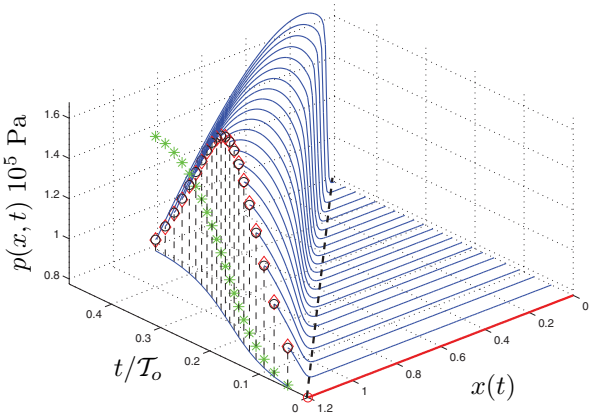

(c) $f_o = 159$ Hz, $\Delta M_f/M_f(0) = 0.08\%$.

Fig. 7.3 *3D view of pressure changes during half a period:* $u^0 = 0.2$ *m,* $\mathcal{F}_o = 2.10^6$ *N.*

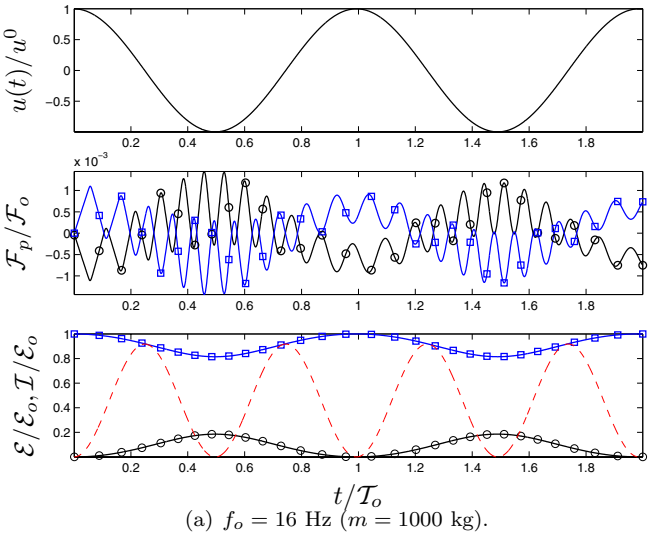

(a) $f_o = 16$ Hz ($m = 1000$ kg).

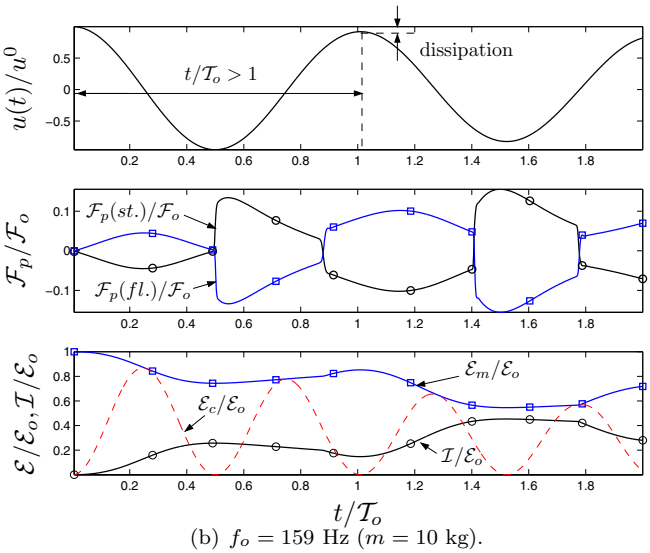

(b) $f_o = 159$ Hz ($m = 10$ kg).

Fig. 7.4 *Piston motion, force, and energy transfer signals vs. time during two natural periods (□ symbols are relative to the fluid and ∘ symbols are relative to the structure).*

Computing time is equal to twice the natural period of the piston ($t_{max} = 2 \times \mathcal{T}_o$). We observe the following:

1. The piston force evolutions (middle graphs), resulting from both the fluid momentum integration (5.2) and the fluid pressure, perfectly correspond. One is the inverse of the other, owing to opposite normals on the piston (action-reaction principle).
2. Energy conservation (bottom graphs) is always ensured and the difference between mechanical energy and impulsion remains lower than 0.1% throughout. They move in opposite directions, showing that *what is lost* by one is *taken back* by the other.

3. In all cases, the mechanical energy (lower graphs) does not remain constant, indicating that energy is transferred from the piston to the fluid. A small dissipative effect is visible in the highest frequency case attenuating the $u(t)$ signal. This shows a strong coupling between the fluid and the piston.
4. In Figure 7.4 (b) (top graph), we observe that the period of the piston is greater than its natural period $\mathcal{T}_o$. This demonstrates that FSI may change the dynamic behavior of a flexible structure (*aeroelasticity* domain [4]).

7.3. Comparing the ALE, Eulerian, and Lagrangian Approaches. We comment on results obtained using the following derivative versions of the C-model:

1. An ALE approach.
2. A *Lagrangian* approach, where $w_x(x,t) = v(x,t)$ (see Remark 3).
3. A pure *Eulerian* approach, where $w_x(x,t) = 0$, completed with a mesh deformation.

REMARK 6. *The third version (pure Eulerian on a moving mesh) illustrates the error to be avoided and corresponds to the direct use of a classical compressible fluid flow solver on a movable mesh with no flux correction.*

Piston pressure evolutions are plotted in Figure 7.5 (a) and (b), respectively, for $f_o = 50$ and 159 Hz. The solution obtained via the Eulerian approach is depicted with dashed lines. The results of the ALE and Lagrangian approaches perfectly match (equivalent to results shown in Figures 7.1 (b) and (c)); this means that the solution is not mesh velocity dependent.

We observe that the Eulerian approach always overestimates the change in piston pressure, as long as there is no reflective wave.

This overestimation may be greater than 80%. Moreover, it does not by any means guarantee the conservation of total fluid mass, which may increase by as much as 67%, whereas it is lower than 0.1% for the ALE and the Lagrangian approaches. It can be seen that a sharp time step reduction has no significant corrective effect for the Eulerian approach, and that a reduction in mesh size (increasing *Nelt*) leads to worse results, because node traversing effects become more significant as *Nelt* increases. The ALE and Lagrangian models give similar results. The choice between them will be determined by the domain characteristics, open or closed. In most cases the ALE approach is preferable, since a Lagrangian approach used in an open domain (with

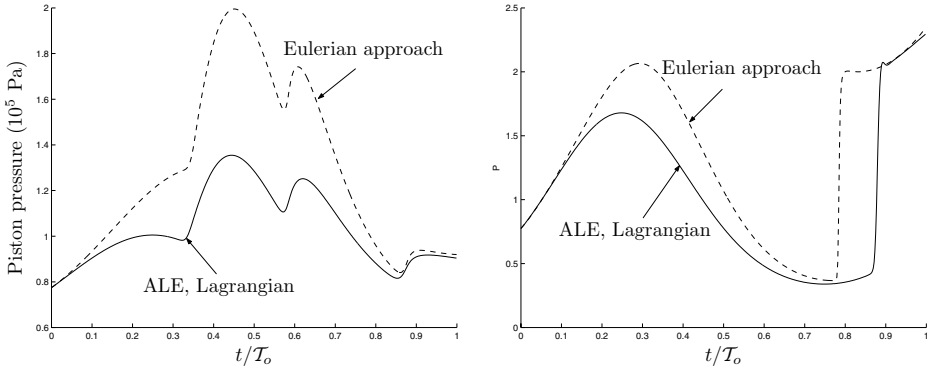

(a) $f_o = 50Hz$: $\Delta M_f/M_f(0) = 49\%$. (b) $f_o = 159Hz$: $\Delta\ M_f/M_f(0) = 67\%$.

Fig. 7.5 *Comparative profiles: ALE (straight lines) vs. Eulerian approach (dashed lines).*

flow inlet and outlet) will always lead to severe mesh distortions, even though the Lagrangian approach is suitable for a closed domain.

8. Conclusions. This introduction to fluid-structure computation uses the example of a gas contained in a 1D chamber closed by a moving piston. Only one model is proposed for the piston dynamics. This *simple* textbook case allows us to introduce three different fluid models of increasing accuracy and complexity: a stationary analytical model (A-model), an exact wave model for piston pressure calculation (B-model), and a complete 1D compressible fluid flow model (C-model).

It is shown that the simplest A-model is only suitable for low frequency responses of the piston that lead to a quasi-steady-state evolution of the fluid.

For higher frequencies, the exact B-model is the best choice only for *semi-infinite* chambers (no reflective wave), but this model only gives the pressure on the piston.

The C-model is the most complex and complete model. It offers a good approximation of the pressure and fluid velocity at any point in the domain and at any time step. The notion of movable domain is considered in order to take account of changes in chamber length resulting from piston motion, which gives rise to the general ALE approach in addition to the classical Lagrangian and Eulerian approaches. Three criteria are described, respectively, for mass, momentum, and energy, as a means of checking the conservation capability of the ALE approach and of the coupling scheme between the fluid and the structure. It is shown that the C-model, using a pure Eulerian approach and with a moving mesh adaptation, yields only unsatisfactory results, with pressure being overestimated and with no guarantee of mass conservation.

For readers interested in extending this 1D approach to 2D and 3D models, we now provide a nonexhaustive list of important requirements for high-quality coupling calculations:

1. The use of a technique to automatically compute the deformation of the fluid mesh at each new time step. We generally consider a pseudomaterial analogy for the fluid mesh that can be deformed using classical elasticity problem solvers [26, 28].
2. Respect of a *space conservation law* for the fluid model in 2D or 3D. For example, in 2D, this stipulates that the update of the solution from time n to time $n+1$ requires the integration of the fluid flow equations on the intermediate mesh given at time $n+1/2$ (see [9, 12, 16, 29] for comprehensive details).
3. The coupling scheme should require a *subcycling* approach in order to update the structure deformation only after N_f fluid time step calculations, for reasons of time efficiency. This implies modifying the coupling scheme by introducing an iterative procedure.
4. The quality of the coupling should be measured during a postprocessing phase to ensure mass, momentum, and energy conservation at each time step between the fluid domain and the structure.
5. In order to facilitate the computing implementation, the use of a parallel environment with *message passing* capabilities, such as PVM [14] or MPI [22], is recommended.

Notation.

$\{.\}$	: column vector
$\langle . \rangle$	: row vector
$[.]$	: matrix
$.^0$	: initial at time $t = 0$
$._o$	: at rest
$.(x,t)$	: x- and t-dependent
ξ	: reference space
j	: node index
$n{-}1, n, n{+}1$	: indices for time steps $t - \Delta t$, t, and $t + \Delta t$

Structure Nomenclature.

A	: piston area	[m^2]
m_p	: piston mass	[kg]
k_p	: spring rigidity	[N/m]
$L_{so}, L_{se}, L_s(t)$	: spring length unstretched, at rest, and at time t	[m]
$u(t), \dot{u}(t), \ddot{u}(t)$	: piston displacement, velocity, and acceleration	[m, m/s, m/s^2]
$\vec{n}$	: normal vector to the piston	
f_o, $\mathcal{T}_o$	: natural frequency and period of the mass-spring	[Hz], [s]
Δt	: time step	[s]
$\mathcal{E}, \mathcal{E}_c, \mathcal{E}_p$	: mechanical, kinetic, and potential energies	[J]

Fluid Nomenclature.

$\rho(t)$	: volumic mass	[kg/m^3]
p	: pressure	[Pa]
v	: fluid velocity	[m/s]
c	: speed of sound	[m/s]
J	: Jacobian	
L	: chamber length	[m]
w_x	: nodal mesh velocity	[m/s]
e	: total volumic energy	[J]
C_v	: specific heat capacity	[$m^2 s^{-2} K^{-1}$]
$\mathcal{R}$	: individual gas constant	[$m^2 s^{-2} K^{-1}$]
T	: temperature	[K]
V	: chamber volume	[m^3]
γ	: specific ratio of the air	
$F_i(q)$	: flux term of quantity q	[q × m^3/s]
$\tilde{F}_i(q)$	: corrected flux term of quantity q	[q × m^3/s]
$\mathcal{I}$	: impulsion	[J]

REFERENCES

[1] *Numerical Recipes in Fortran: The Art of Scientific Computing*, Cambridge University Press, Cambridge, UK, 1992.

[2] H. Ashley and G. Zartarian, *Piston theory—a new aerodynamic tool for the aeroelastician*, J. Aeronaut. Sci., 23 (1956), pp. 1109–1118.

[3] A. Beiser, *Applied Physics*, McGraw–Hill, New York, 2004.

[4] R. L. Bisplinghoff and H. Ashley, *Principles of Aeroelasticity*, John Wiley and Sons, New York, 1975.
[5] J. P. Boris and D. L. Book, *Flux-corrected transport.* I. *SHASTA, a fluid transport algorithm that works*, J. Comput. Phys., 135 (1997), pp. 172–186.
[6] R. Bronson, *Schaum's Outline of Theory and Problems of Matrix Operations*, McGraw–Hill, New York, 1988.
[7] R. Bronson and G. Costa, *Schaum's Outline of Differential Equations*, McGraw–Hill, New York, 2006.
[8] G. Buchanan, *Finite Element Analysis*, McGraw–Hill, New York, 1995.
[9] I. Demirdzic and M. Peric, *Space conservation law in finite volume calculations of fluid flow*, Internat. J. Numer. Methods Fluids, 8 (1988), pp. 1037–1050.
[10] G. Dhatt, G. Touzot, and E. Lefrançois, *Méthode des éléments finis*, Hermès-Lavoisier, 2005.
[11] J. Donea, S. Giuliani, and J. P. Halleux, *An arbitrary Lagrangian-Eulerian finite element method for transient dynamic fluid-structure interactions*, Comput. Methods Appl. Mech. Engrg., 33 (1982), pp. 689–723.
[12] C. Farhat, P. Geuzaine, and C. Grandmont, *The discrete geometric conservation law and the nonlinear stability of ALE schemes for the solution of flow problems on moving grids*, J. Comput. Phys., 174 (2001), pp. 669–694.
[13] S. J. Farlow, *Partial Differential Equations for Scientists and Engineers*, John Wiley and Sons, New York, 1982.
[14] A. Geist, A. Beguelin, J. Dongarra, W. Jiang, R. Manchek, and V. Sunderam, *PVM* 3 *User's Guide and Reference Manual*, Tech. report, Oak Ridge National Laboratory, 1994.
[15] M. Géradin and D. Rixen, *Mechanical Vibrations: Theory and Applications to Structural Dynamics*, John Wiley and Sons, New York, 1997.
[16] H. Guillard and C. Farhat, *On the significance of the geometric conservation law for flow computations on moving meshes*, Comput. Methods Appl. Mech. Engrg., 190 (2000), pp. 1467–1482.
[17] G. P. Guruswamy, *A review of numerical fluids/structures interface methods for computations using high-fidelity equations*, Comput. & Structures, 80 (2002), pp. 31–41.
[18] S. Kelly, *Schaum's Outline of Engineering Mechanics*, McGraw–Hill, New York, 1999.
[19] S. Kelly, *Schaum's Outline of Theory and Problems of Mechanical Vibrations*, McGraw–Hill, New York, 2008.
[20] P. D. Lax and B. Wendroff, *Systems of conservation laws*, Comm. Pure Appl. Math., 13 (1960), pp. 217–237.
[21] H. W. Liepann and A. Roshko, *Elements of Gasdynamics*, John Wiley and Sons, New York, 1957.
[22] S. Otto, S. Huss-Lederman, D. Walker, J. Dongarra, and M. Snir, *MPI: The Complete Reference*, Vols. 1 and 2, MIT Press, Cambridge, MA, 1998.
[23] S. Piperno, *Staggered Time Integration Methods for a One-Dimensional Euler Aeroelastic Problem*, Tech. report, CERMICS, INRIA, Sophia-Antipolis, France, 1994.
[24] M. Potter and C. Somerton, *Schaum's Outline of Thermodynamics for Engineers*, McGraw–Hill, New York, 2006.
[25] M. Potter and D. Wiggert, *Schaum's Outlines Fluid Mechanics*, McGraw–Hill, New York, 2007.
[26] J. W. Slater, M. S. Liou, and R. G. Hindman, *Approach for dynamic grids*, AIAA J., 33 (1995), pp. 63–68.
[27] M. Spiegel, *Schaum's Outline of Calculus of Finite Differences and Difference Equations*, McGraw–Hill, New York, 1999.
[28] K. Stein, T. E. Tezduyar, and R. Benney, *Mesh moving techniques for fluid-structure interactions with large displacements*, ASME, 70 (2003), pp. 58–63.
[29] P. D. Thomas and C. K. Lombard, *Geometric conservation law and its application to flow computations on moving grids*, AIAA J., 17 (1979), pp. 1030–1037.
[30] O. C. Zienkiewicz and R. L. Taylor, *The Finite Element Method, Vol.* 1: *The Basis*, 5th ed., Butterworth-Heinemann, Oxford, 2000.
[31] O. C. Zienkiewicz and R. L. Taylor, *The Finite Element Method, Vol.* 2: *Solid Mechanics*, 5th ed., Butterworth-Heinemann, Oxford, 2000.
[32] O. C. Zienkiewicz and R. L. Taylor, *The Finite Element Method, Vol.* 3: *Fluid Dynamics*, 5th ed., Butterworth-Heinemann, Oxford, 2000.